Dierk Raabe, Frank Heringhaus[1], Ude Hangen and Günter Gottstein

(Institut für Metallkunde und Metallphysik, Kopernikusstr. 14, Rheinische-Westfälische Technische Hochschule Aachen, D-52056 Aachen, Germany)

Investigation of a Cu-20 mass% Nb in situ Composite, Part II: Electromagnetic Properties and Application

Fiber or ribbon reinforced in situ metal matrix composites (MMCs) consisting of Cu and 20 mass% Nb were produced by large strain wire drawing and cold rolling of a cast ingot. The microstructure of the composites was studied by use of scanning and transmission electron microscopy. The normal and superconducting properties of the wires and sheets in the presence of externally imposed magnetic fields were investigated and compared with the electromagnetic properties of pure Cu and Nb. The observations are discussed in terms of the microstructural changes during wire drawing and rolling. The current results substantiate that the amount of internal phase boundaries and the filament spacing have considerable influence on the normal and superconducting properties of Cu-20 mass% Nb. On the basis of the current findings potential industrial applications are discussed.

Untersuchung eines Cu-20 Masse-% Nb in situ Verbundwerkstoffes
Teil II: Elektromagnetische Eigenschaften und Anwendungen

Faserverstärkte in situ Metallmatrix-Verbundwerkstoffe (MMCs) bestehend aus Cu und 20 Masse-% Nb wurden durch starke Draht- sowie Walzverformung aus einem Gussblock hergestellt. Die Mikrostrukturentwicklung des Verbundwerkstoffes wurde mittels Raster- und Transmissionselektronenmikroskopie untersucht. Die normal- und supraleitenden Eigenschaften der Drähte und Bleche wurden unter dem Einfluß äußerer magnetischer Felder gemessen und mit den elektromagnetischen Eigenschaften von reinem Cu und Nb verglichen. Die ermittelten Daten werden auf der Basis der mikrostrukturellen Entwicklung im Verlauf des Walzens und Drahtziehens diskutiert. Die vorliegenden Ergebnisse belegen, daß der Anteil an inneren Phasengrenzflächen und der Faserabstand einen beträchtlichen Einfluß auf die normal- und supraleitenden Eigenschaften von Cu-20 Masse-% Nb haben. Auf der Basis der gegenwärtigen Resultate werden potentielle industrielle Anwendungen erörtert.

1 Introduction

Cu and Nb have no mutual solubility by practical standards [1]. Therefore, fiber or ribbon reinforced in situ MMCs can be manufactured by large degrees of deformation, e.g. by wire drawing or rolling of a cast ingot [2 to 8]. Heavily deformed Cu–Nb MMCs reveal a very high strength and good electrical conductivity [2 to 17]. Whereas the fabrication, the microstructure and the resulting mechanical properties of Cu-20 mass% Nb have been subject to part I of this study [18], part II is primarily concerned with the investigation of the normal and superconducting properties of rolled and wire drawn specimens in the presence of external magnetic fields. On the basis of the microstructural data discussed in part I a simulation of the normal-state resistivity of Cu-20 mass% Nb is carried out which accounts for the inelastic scattering of conduction electrons at phase boundaries and dislocations. Finally, potential industrial applications are discussed.

2 Electromagnetic Properties

2.1 Experimental and Results

The resistivity measurements on rolled and wire drawn specimens were carried out by means of the DC four-probe technique using currents within the range 10 to 100 mA. For the investigation of the normal and superconducting properties under externally imposed magnetic fields up to 15 Tesla, an Oxford Instruments superconducting magnet was employed. The measurements were executed within the temperature range 3 K to 300 K. A set of two samples, i.e. Cu and Cu-20 mass% Nb having the same degree of deformation, were positioned in the center of the superconducting magnet in such a way that the direction of the external magnetic force was perpendicular to the current flow in the samples. The data were taken continuously during cooling. Details of the experimental technique are discussed elsewhere [17].

Measurements of the electrical resistivity were conducted at 295 K, 198 K and 77 K (Fig. 1). A typical dependence of the resistivity of both pure Cu (open symbols) and of Cu-20 mass% Nb (filled symbols) at these temperatures is shown for the wire drawn samples in Fig. 1a and for the cold rolled specimens in Fig. 1b. The resistivity of pure Cu appears to be independent of the degree of deformation (Fig. 1). The resistivity of Cu-20 mass% Nb was always larger than for pure Cu and increased for $\eta > 6$ ($\varepsilon = 99.75\,\%$) in case of wire and for $\eta > 3$ ($\varepsilon = 95\,\%$) in case of sheet material. The measurements were repeated after a heat treatment of 5 h at 823 K (Fig. 2). Within the resolution of the technique used, the resistivity of pure Cu was nearly not affected by such annealing, but the resistivity

[1]) now with: National High Magnetic Field Laboratory, Tallahassee, Florida 32306, USA

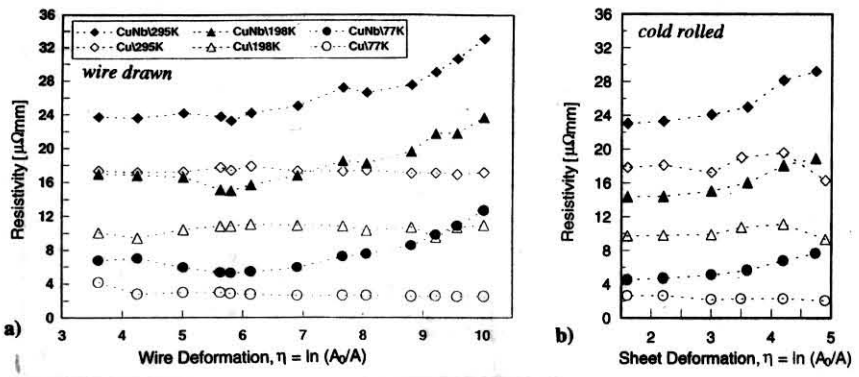

Fig. 1a and b. Resistivity of Cu and Cu-20 mass% Nb with progressing deformation for three different temperatures. a) Wire drawn samples. b) Cold rolled samples.

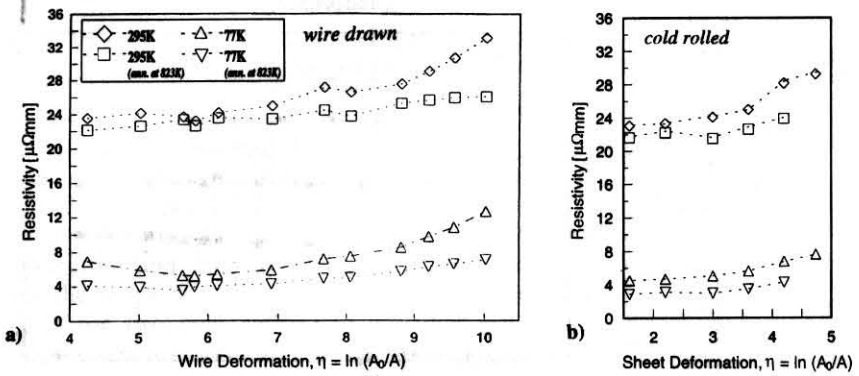

Fig. 2a and b. Resistivity of Cu-20 mass% Nb with progressing deformation measured at two different temperatures, with and without heat treatment at 823 K for 5 h. a) Wire drawn samples. b) Cold rolled samples.

of Cu-20 mass% Nb noticeably decreased. This drop of the resistivity was uniform up to about $\eta = 6$ ($\varepsilon = 99.75\,\%$) for wires (Fig. 2a) and $\eta = 3$ ($\varepsilon = 95\,\%$) (Fig. 2b) for sheets and became more pronounced with increasing deformation.

Fig. 3 shows the change of the specific magnetoresistance of maximum deformed (wire drawn) Cu and Cu-20 mass% Nb samples ($\eta = 10$, $\varepsilon = 99.995\,\%$) as a function of the external magnetic field. Without magnetic field the residual resistivity amounted to $\varrho_{Cu(4.2\,K)} = 0.4\ \mu\Omega$ mm for pure Cu (Fig. 4a) and $\varrho_{Cu\text{-}Nb(4.2\,K)} = 9\ \mu\Omega$ mm for Cu-20 mass% Nb (Fig. 4b). The residual resistivity ratio for pure Cu was $\varrho_{295\,K}/\varrho_{4.2\,K} = 48$ which is lower than expected from the initial purity of 99.99 mass%. It is hence assumed that during melting and casting the impurity content was augmented. The resistivity of pure, wire drawn Cu did not

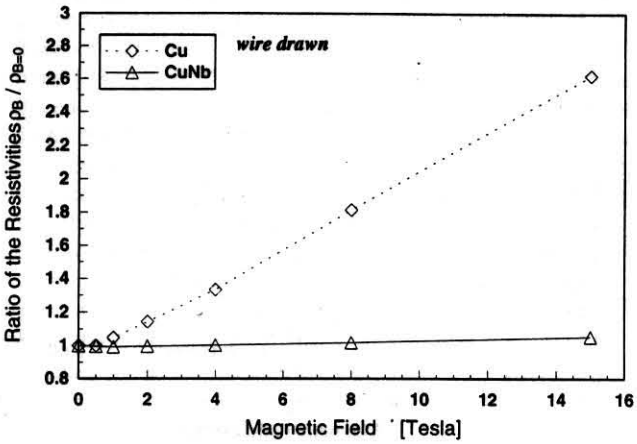

Fig. 3. Normalized resistivity $\varrho(B)/\varrho(B = 0)$ of wire drawn Cu and Cu-20 mass% Nb ($\eta = 10$, $\varepsilon = 99.995\,\%$) exposed to a magnetic field B.

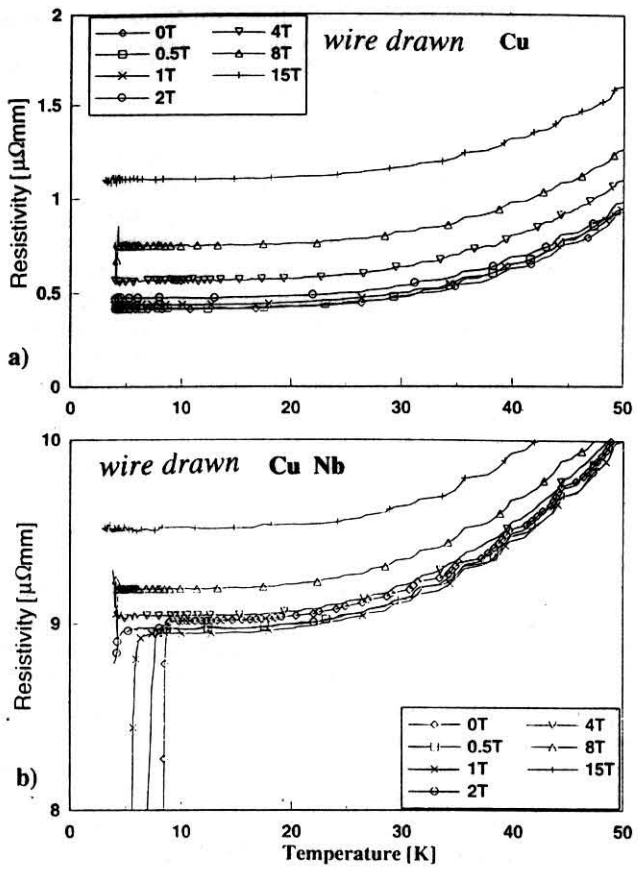

Fig. 4a and b. Temperature dependent resistivity of wire drawn Cu and Cu-20 mass% Nb for different externally imposed transverse magnetic fileds ($\eta = 10$, $\varepsilon = 99.995\,\%$). a) Cu, b) Cu-20 mass% Nb.

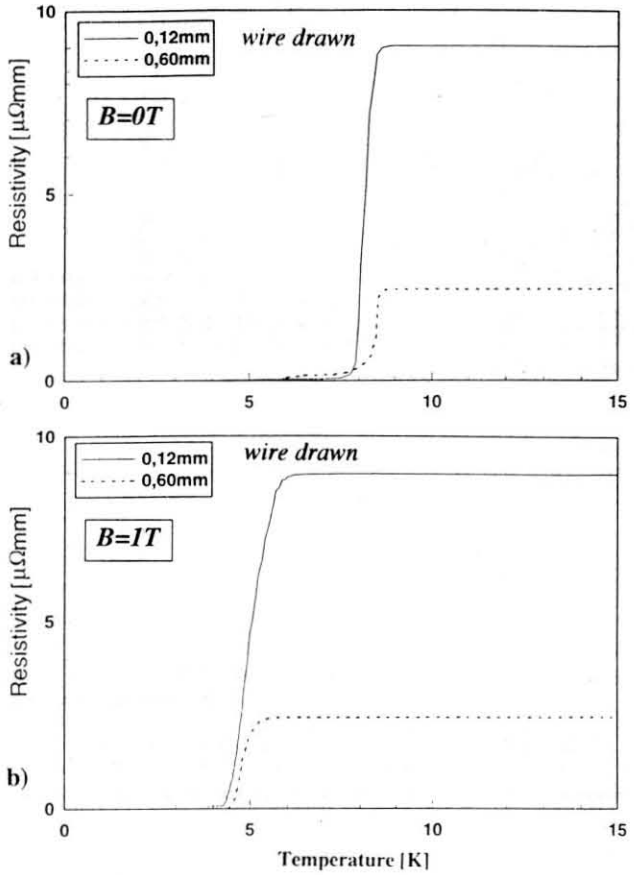

Fig. 5a and b. Resistivity of wire drawn Cu-20 mass% Nb as a function of the temperature for two different degrees of deformation ($d = 0.6$ mm [$\eta = 6.8$, $\varepsilon = 99.89$ %]; $d = 0.12$ mm [$\eta = 10$, $\varepsilon = 99.995$ %]). a) $B = 0$ T, b) $B = 1$ T.

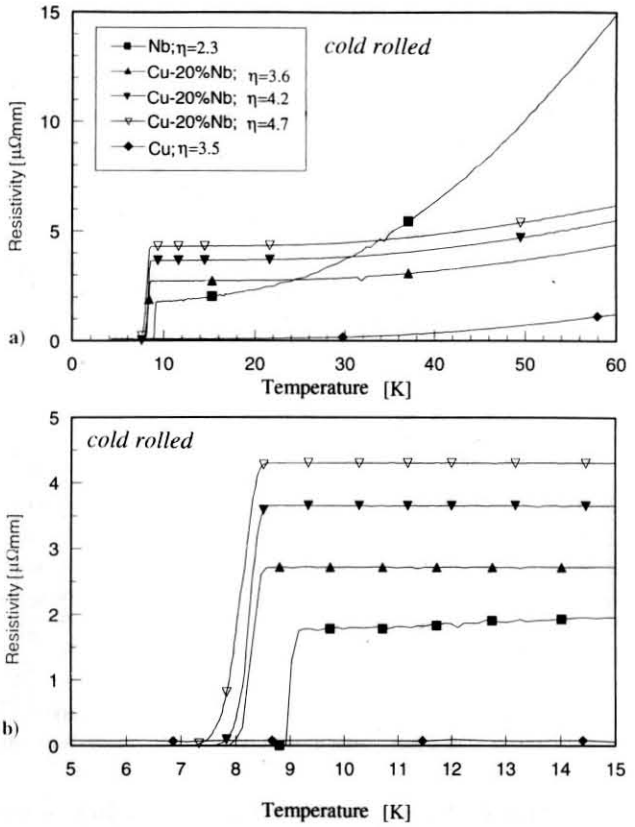

Fig. 6. Resistivity of cold rolled pure Cu, pure Nb and Cu-20 mass% Nb (three different degrees of deformation, $\eta = 3.6$ ($\varepsilon = 97.268$ %), $\eta = 4.2$ ($\varepsilon = 98.500$ %), $\eta = 4.7$ ($\varepsilon = 99.09$ %) as a function of the temperature.

change significantly up to weak transverse magnetic fields, of 2 T, but at higher fields a considerable increase was observed. This effect became especially apparent at low temperatures. An external field of 15 T increased the residual resistivity of pure Cu at 4.2 K by $\Delta\varrho = 0.7$ μΩ mm. A similar behavior was found for Cu-20 mass% Nb. Up to 4 T no significant contribution of the magnetic field on resistivity was observed. At a magnetic field force of 15 T, however, the resistivity was raised by $\Delta\varrho = 0.5$ μΩ mm. Without an external magnetic field the transition from the normal into the superconducting state is found for Cu-20 mass% Nb at about 8 K (Fig. 4b). With increasing magnetic field the corresponding transition temperature was observed to decrease. The same behavior was found for rolled specimens.

As is shown in Fig. 5 for wire drawn Cu-20 mass% Nb, the transition of the superconducting state depended on the degree of deformation, i.e. on the microstructure. With and without applied external magnetic field the resistivity in the normal conducting state was higher for the sample which had undergone a larger thickness reduction. However, both samples revealed the same onset temperature. An external transverse magnetic field led to a decrease of the critical temperature for both levels of deformation and to a shift of the curves relative to each other (Fig. 5b). The onset temperature at $B = 1$ T for the more strongly deformed wire ($d = 0.12$ mm, $\eta = 10$, $\varepsilon = 99.995$ %) was approximately 6 K, and for the less deformed wire ($d = 0.6$ mm, $\eta = 6.8$, $\varepsilon = 99.89$ %) about 5.3 K. Another difference in the transition to the superconducting state at $B = 1$ T as opposed to $B = 0$ T was the larger gap between T_{onset} and T_{offset} ($\Delta T \approx 1$ K for $B = 0$ T, $\Delta T \approx 1.7$ K for $B = 1$ T, e.g. for $d = 0.12$ mm). The same results were found for rolled specimens. In Fig. 6 the dependence of the onset temperature on the degree of deformation is shown for pure Cu, Cu-20 mass% Nb and for pure Nb. A sweep of the magnetic field at 4.3 K also revealed a difference in the transition to

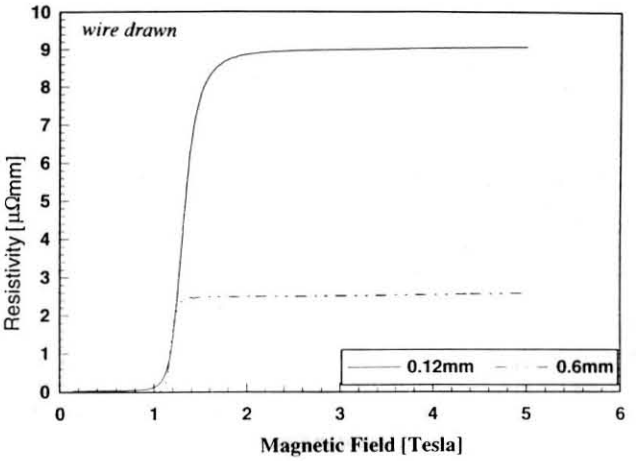

Fig. 7. Resistivity of wire drawn Cu-20 mass% Nb with increasing magnetic field strength for two different degrees of deformation ($d = 0.6$ mm [$\eta = 6.8$, $\varepsilon = 99.89$ %]; $d = 0.12$ mm [$\eta = 10$, $\varepsilon = 99.995$ %]), $T = 4.3$ K.

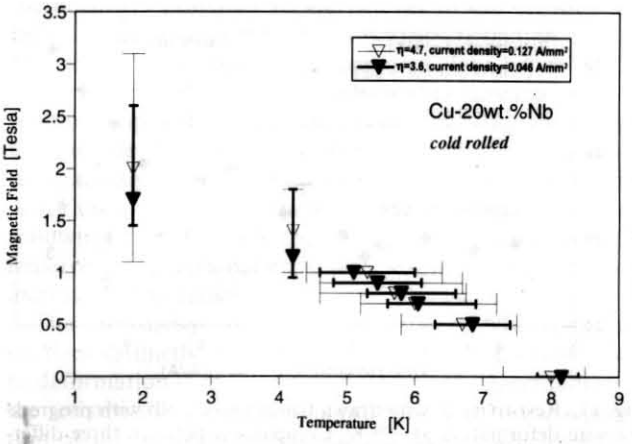

Fig. 8. Magnetic field of a cold rolled Cu-20 mass% Nb superconductor as a function of the critical temperature, $\eta = 3.6$ ($\varepsilon = 97.268\,\%$) and $\eta = 4.7$ ($\varepsilon = 99.09\,\%$).

the resistive state for both levels of deformation. The wire drawn sample with $\eta = 6.8$ ($\varepsilon = 99.89\,\%$) required a critical field of about $B = 1.3$ T, while the specimen with $\eta = 10$ ($\varepsilon = 99.995\,\%$) needed almost $B = 2$ T (Fig. 7). The critical temperature and the critical magnetic field force, which limit the range of the superconducting state, are given in Fig. 8 for two cold rolled samples. The same kind of behavior was found for wire drawn specimens.

2.2 Simulation of the Resistivity

The experimentally observed degradation of the electrical conductivity was simulated by assuming inelastic scattering of conduction electrons at internal phase boundaries as primary and scattering at dislocations as secondary contribution to the total resistivity of the composite. In the present study the simulations are exemplarily carried out for wire drawn samples.

The mean free path of a conduction electron in pure Cu was estimated theoretically [19] and confirmed experimentally [20, 21] as $l = 43$ to 45 nm at 293 K, $l = 61$ to 63 nm at 198 K and $l = 138$ to 145 nm at 77 K. As suggested from experimental data, the mean free electron path in Nb was assumed as $l = 3.1$ nm at 293 K, $l = 5$ nm at 198 K and $l = 17.6$ nm at 77 K [22]. For a quantitative assessment of the dependence of resistivity upon fiber geometry in the deformed MMC, the theory of electron scattering at the surface of very thin wires, referred to as size effect, was applied [23, 24]. In the present approach the free surface is replaced by the internal boundary between the Cu matrix and the Nb filaments. The two phases hence represent two linear resistors connected parallel, the resistivity of each varies according to their filament thickness. For the sake of simplicity, the Nb filament spacing is identified with the thickness of the Cu filaments. The corresponding data are available from experiments which were presented in part I of this study. The resistivity of either phase can then be determined according to [23]:

$$\varrho(d) = \varrho_0\left(1 + \frac{3}{4}(1-p)\frac{l_0}{d}\right) \tag{1}$$

where $\varrho(d)$ is the resistivity as a function of the filament thickness, ϱ_0 the resistivity for a sample without scattering at the phase boundary, l_0 the mean free path of a conduction electron, and d the thickness of the fiber. The factor $(1-p)$ represents the probability of inelastic scattering [23]. According to investigations on Cu–Nb it was estimated that p is close to 0 [21]. The approach suggested in Eq. (1) is usually applied for $d > l_0$. This condition holds for the Cu ($d_{Cu}/l_{0\,Cu} \approx 3$) as well as for the Nb phase ($d_{Nb}/l_{0\,Nb} \approx 20$) corresponding to the current data for $\eta = 10$ ($\varepsilon = 99.995\,\%$) and $T = 293$ K (wire). Assuming inelastic scattering, Eq. (1) results in:

$$\varrho_{Cu}(d_{Cu}, T) = \varrho_{Cu0}(T) \cdot \left(1 + \frac{3}{4} \cdot \left(\frac{l_{Cu}(T)}{d_{Cu}}\right)\right) \tag{2}$$

The same relation also holds for the Nb phase. Here $\varrho_{Cu}(d_{Cu}, T)$ (and $\varrho_{Nb}(d_{Nb}, T)$) are the resistivities of Cu (and Nb) as a function of fiber diameter and temperature, in case that only inelastic scattering is taken into account. In part I of this study [18] it was shown that after heavy deformation the morphology of both phases is no longer cylindrical, but curled. Hence, a correction term which accounts for the curled morphology, is introduced.

$$\varrho_{Cu}(d_{Cu}, T) = \varrho_{Cu0}(T) \cdot \left(1 + \frac{3}{4} \cdot \left(\frac{l_{cu}(T)}{d_{Cu} \cdot \left(1 - 0.44 \cdot \left(\frac{\eta}{\eta_{max}}\right)\right)}\right)\right) \tag{3}$$

Incorporating additionally the resistivity which is contributed by the increasing dislocation density, $\Delta\Lambda$, in both phases, Eq. (3) can be written as

$$\varrho_{Cu}(d_{Cu}, T) = \varrho_{Cu0}(T) \cdot \left(1 + \frac{3}{4} \cdot \left(\frac{l_{Cu}(T)}{d_{Cu} \cdot \left(1 - 0.44 \cdot \left(\frac{\eta}{\eta_{max}}\right)\right)}\right)\right) + \Delta\Lambda_{Cu} \cdot \varrho_{Cu_{Disloc}}. \tag{4}$$

Equations (2) to (4) equivalently hold for the resistivity of the Nb phase. On Cu numerous investigations have been carried out in order to measure the contribution of dislocations to the total resistivity [e.g. 25, 26]. According to these works a dislocation resistivity of $\varrho_{Cu.Disloc.} = 2 \cdot 10^{-26}\ \Omega m^3$ is used in the present calculation. In case of Nb, however, no reliable data on the contribution of dislocations to the total resistivity are available. For supplying adequate data, hence the development of the resistivity of a pure Nb specimen as a function of strain was examined experimentally. For this purpose pure Nb specimens were cold rolled to a true strain

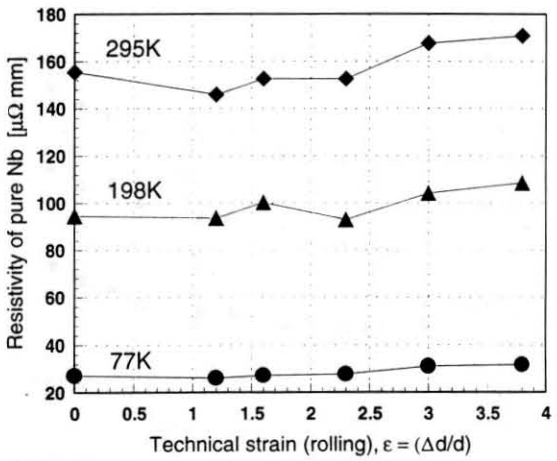

Fig. 9. Increase of the resistivity of cold rolled pure Nb as a function of the deformation.

of $\eta = 4$ ($\varepsilon = 98.17\,\%$). As is evident from Fig. 9, the resistivity of the pure Nb samples revealed a stronger increase with deformation than the Cu specimens (Fig. 1). For providing a lower bound estimation of the resistivity contributed by dislocations, it was assumed that the dislocation density in the cold rolled Nb samples increased from $10^{10}\,m^{-2}$ to $10^{16}\,m^{-2}$. According to Fig. 9, a contribution of $\varrho_{Nb,Disloc.} = 25 \cdot 10^{-24}\,\Omega m^3$, which considerably exceeds the value for Cu, is thus suggested. The high resistivity contribution of dislocations in Nb is attributed to the three-dimensional core geometry of the bcc screw dislocations and – to a certain extent – also of the 71° edge dislocations. In the current model, the dislocation density in both phases, Λ, was assumed to increase linearly with the technical strain ε.

For the pure and undeformed constituents, Cu and Nb, the following resistivities were measured on bulk samples: $\varrho_{Cu0} = 17\,\mu\Omega\,mm$ and $\varrho_{Nb0} = 155\,\mu\Omega\,mm$ at 295 K, $\varrho_{Cu0} = 10\,\mu\Omega\,mm$ and $\varrho_{Nb0} = 95\,\mu\Omega\,mm$ at 198 K as well as $\varrho_{Cu0} = 3\,\mu\Omega\,mm$ and $\varrho_{Nb0} = 27\,\mu\Omega\,mm$ at 77 K. On the basis of the microstructural data the evolution of the filament thickness with increasing wire deformation was described by the following expressions:

$$d_{Cu}(\eta) = d_{Cu}(0) - k_{Cu} \cdot \ln(\eta) \quad d_{Nb}(\eta) = d_{Nb}(0) - k_{Nb} \cdot \ln(\eta) \tag{5}$$

where $d_{Cu}(\eta)$ is the thickness of the Cu and $d_{Nb}(\eta)$ that of the Nb filaments for a wire deformation η. The experimental results can be fitted in the range, $1 \leq \eta \leq 10$ ($\varepsilon = 63.212\,\%$ to $\varepsilon = 99.995\,\%$), by $d_{Cu}(0) = 3609.51$ nm, $k_{Cu} = 1504.25$ nm, $d_{Nb}(0) = 1855.50$ nm and $k_{Nb} = 774.98$ nm. According to the approach of parallel connected resistors, the total resistivity ϱ then depends on ϱ_{Cu} and ϱ_{Nb} as

$$\frac{1}{\varrho} = \frac{0.8}{\varrho_{Cu}} + \frac{0.2}{\varrho_{Nb}} \tag{6}$$

2.3 Discussion

The results of the simulations are together with the experimentally detected normal-state resistivities depicted in Fig. 10 for three various temperatures (wire drawn samples). The evolution of the resistivity, i.e. especially the experimentally observed increase at large strains is adequately covered by the model. As a result, the increase of resistivity in largely strained MMCs can essentially be attributed to

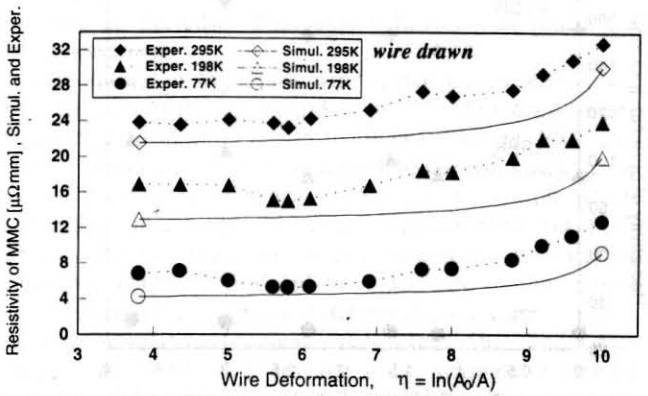

Fig. 10. Resistivity of wire drawn Cu-20 mass% Nb with progressing wire deformation for three different temperatures. Comparison between experimentally determined and simulated data.

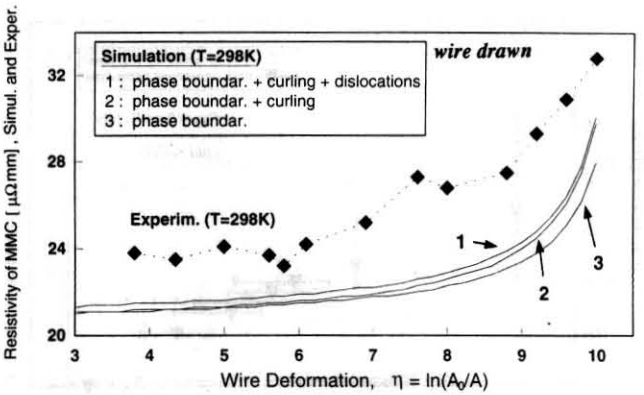

Fig. 11. Resistivity of wire drawn Cu-20 mass% Nb with progressing wire deformation at 298 K. Comparison between three different contributions: (1) Inelastic scattering at phase boundaries + curled filament geometry + dislocations; (2) inelastic scattering at phase boundaries + curled filament geometry; (3) inelastic scattering at phase boundaries only.

scattering of conduction electrons at phase boundaries. However, two deviations from the experimental findings are apparent. First, the calculated resistivities are somewhat lower than the experimental ones. Second, the weak drop of the resistivity which was observed within the range $5 < \eta < 7$ ($\varepsilon = 99.33\,\%$ to $\varepsilon = 99.91\,\%$), especially at 77 K and 198 K, is not covered by the model. It appears likely that the first deviation is due to the microstructural data which the current simulation is based upon. It was reported by Verhoeven et al. [27] that transmission electron microscopy (TEM) has to be employed in order to painstakingly record filament diameter and spacing also for heavily deformed Cu–Nb MMCs. It has thus to be taken into consideration that the experimentally observed average fiber data used for the fit procedure are somewhat too large. If the increase of the resistivity is entirely attributed to inelastic scattering of electrons at phase boundaries, a fiber spacing of about 51 nm rather than of 130 nm is suggested by the experimental results. Furthermore, the real morphology and thus also the true amount of the phase boundaries is much more intricate than suggested by the here employed simplified fitting parameters. Although the correction term used accounts in a simplified manner for the curled boundary geometry, it appears that a more appropriate description has to be deduced. Albeit incorporated in the simulation, inelastic scattering at dislocations is considered to be of minor relevance. The two latter explanations given for the deviations observed were also quantitatively examined. As is evident from Fig. 11, the inelastic scattering of conduction electrons owing to both, the enhancement of the internal phase boundary area (curling) and the increase of the dislocation density is indeed of minor impact on the total normal-state resistivity. It is hence confirmed that the determination of the microstructural data is of dominant importance for an adequate simulation and needs to be improved by employing TEM rather than merely SEM measurements. Vice versa it is to say that the measurement of the resistivity provides a useful diagnostic means of quantitatively gauging microstructural data such as the average filament spacing.

The second deviation, i.e. the resistivity drop within the range $5 < \eta < 7$ ($\varepsilon = 99.33\,\%$ to $\varepsilon = 99.91\,\%$), is attributed to the initial rotation of the Nb dendrites. As is evident from the microstructural data, up to $\eta = 6$ ($\varepsilon = 99.75\,\%$),

the dendrites primarily rotate parallel to the drawing axis rather than undergoing large thickness reduction. In this regime the total phase boundary area does hence not increase considerably. However, the scattering cross-sectional fraction imposed by the Nb phase, hindering the current flow in the Cu parallel to the longitudinal direction, is continuously reduced and reaches a minimum when the dendrites are aligned parallel to the drawing axis. In the following, i.e. for $\eta > 6$, the aligned Nb dendrites reveal a massive cross-sectional reduction leading to the observed increase of the resistivity.

The resistivity of the Cu-20 mass% Nb composite changes distinctly on annealing (5 h at 823 K) subsequent to deformation (Fig. 2). At small strains the general drop of the resistivity (≤ 2 μΩ mm) is probably due to the segregation of solute atoms to internal boundaries which serve as sinks. The foreign atoms were presumably of sulfur which might stem from the graphite crucible where they represent the main impurity. Recrystallization of the Cu phase within the MMC is less likely to produce this effect at low strains. The high impurity content of the Cu in the composite is documented by the low value of the residual resistivity ratio which was measured for the pure Cu used to prepare the alloys. At higher degrees of deformation the loss of the resistivity during heat treatment of Cu-20 mass% Nb becomes even more evident (Fig. 2). This drop is likely to be due to coarsening of the Nb filaments since for the diffusion controlled coarsening of the ribbons, mass transport can take place along the Cu–Nb phase boundaries with a much lower energy of activation than for bulk diffusion [28].

3 Applications

Owing to the observed combination of high strength and good electrical conductivity, Cu–Nb based MMCs are considered as candidate materials for the production of highly mechanically stressed electrical devices such as application in long-pulse high-field resistive magnets [11, 29]. The development of such magnets is the subject of considerable research work throughout the world. Induced field strengths in excess of 30 T can be achieved only as pulses generated by the discharge of energy from a capacitor bank into a resistive solenoid. Such applications, however, require two essential properties of the material employed. First, low electrical resistivity to degrade the temperature rise due to flow of current in the coil and second, high mechanical strength to resist the Lorentz forces exerted during the pulse. The potential use of these composites, however, is much more widespread, e.g. applications in electric devices in automobiles, in propulsion systems or as conducting frames in microelectronics are conceivable. By diffusion alloying type II superconductors consisting of a Cu matrix and embedded Nb_3Sn filaments can be fabricated. However, in order to optimize the relation between production costs on the one hand and technical properties on the other hand, it is suggested to concentrate also on the investigation of composites with a content of only 5 to 10 mass% Nb.

4 Conclusions

The normal and superconducting properties and the potential technical applications of heavily rolled and wire drawn Cu-20 mass% Nb in situ composites have been investigated. It was shown that Cu-20 mass% Nb is a material with very high strength and good electrical conductivity. The experimental results were discussed on the basis of the microstructure evolution. The normal-state resistivity of the composite increased with decreasing fiber diameter and filament spacing. This was interpreted in terms of inelastic scattering of the conduction electrons at the phase boundaries. The increase of the contribution of scattering at the internal boundaries with decreasing temperature was interpreted by the growing mean free path of the conduction electrons. The magnetoresistance was found to be larger in pure Cu than in Cu-20 mass% Nb. Also weakly deformed Cu-20 mass% Nb samples show a transition into the superconducting state. It was suggested that weak links occur between the Nb filaments and maintain superconductivity. A corresponding microstructural dependence of the superconductivity was observed. The electrical resistivity was successfully simulated as a function of strain and temperature for the normal conducting regime. Rolled and wire drawn specimens revealed consistent behavior. The current results substantiate that Cu based in situ composites represent a group of materials with a very high potential for various technical applications where a combination of very high mechanical strength and good electrical conductivity is required.

The authors gratefully acknowledge the kind support by the National High Magnetic Field Laboratory in Tallahassee, Florida, where the measurements of the electromagnetic properties were carried out. A portion of this work was supported by NSF Cooperative Agreement No. DMR-9016241 and by the State of Florida. The authors thankfully acknowledge the kind support by Dr. H.-J. Scheider-Muntau, Dr. L. T. Summers and Dr. E. Palm. One of the authors gratefully acknowledges the kind support by the Adolf-Martens-Gesellschaft in Berlin, especially by Prof. Dr. Dr. E.h. W. Dahl and Prof. Dr. Dr. h.c. H. Czichos.

Literature

1. *Chakrabati, D. J.: Laughlin, D. E.:* Bull. Alloy Phase Diagrams *2* (1982) 936.
2. *Karasek, K. R.; Bevk, J.:* J. Appl. Phys. *52* (1981) 1370.
3. *Bevk, J.; Harbison, J. P.; Bell, J. L.:* J. Appl. Phys. *49* (1978) 6031.
4. *Spitzig, W. A.; Pelton, A. R.; Laabs, F. C.:*Acta metall. *35* (1987) 2472.
5. *Spitzig, W. A.:* Acta metall. *39* (1991) 1085.
6. *Trybus, C.; Spitzig, W. A.:* Acta metall. *37* (1989) 1971.
7. *Heringhaus, F.; Raabe, D.; Kaul, L.; Gottstein, G.:* Zeitschrift Metall *6* (1993) 558.
8. *Spitzig, W. A.; Krotz, P.:* Scripta metall. *21* (1987) 1143.
9. *Funkenbusch, P. D.; Courtney, T. H.:* Acta metall. *33* (1985) 913.
10. *Raabe, D.; Hangen, U.:* in: S. I. Andersen, J. B. Bilde-Sorensen, T. Lorentzen, O. B. Pedersen, N. J. Sorensen (eds.), Proc. 15th Risø Int. Symp. on Mat. Sc. on Num. Prediction of Def. Proc. and the Behav. of Real Mat., RISØ Nat. Lab, Roskilde, Denmark (1994) 487.
11. *Embury, J. D.; Hill, M. A.; Spitzig, W. A.; Sakai, Y.:* MRS Bull. *8* (1993) 57.
12. *Schneider-Muntau, H.-J.:* IEEE Trans. Magn. *18* (1982) 32.
13. *Raabe, D.; Gottstein, G.:* J. de Phys. IV, col. C7, sup. J. de Phys. III *3* (1993) 1727.
14. *Heringhaus, F.; Raabe, D.; Gottstein, G.:* Metall *48* (1994) 287.
15. *Raabe, D.;. Heringhaus, F.:* phys. stat. sol. (a) *142* (1994) 473.
16. *Heringhaus, F.; Hangen, U.; Raabe, D.; Gottstein, G.:* Mater. Sci. Forum *157–162* (1994) 709.
17. *Heringhaus, F.; Raabe, D.; Gottstein, G.:* Acta metall., in press.
18. *Raabe, D.; Heringhaus, F.; Hangen, U.; Gottstein, G.:* Z. Metallkd. *86* (1995) 405.
19. *Rider, J. G.; Foxon, C.T.B.:* Phil. Mag. *16* (1967) 1133.

20. *Reynolds, F. W.; Stillwell, G. R.:* Phys. Rev. (1952) 418.
21. *Frommeyer, G.; Wassermann, W.:* phys. stat. sol. (a) *27* (1975) 99.
22. *Auer, J.; Ullmaier, G.:* Phys. Rev. *B7* (1973) 136.
23. *Dingle, R. B.:* Proc. Roy. Soc. London Ser. *201* (1950) 545.
24. *Sondheimer, E. H.:* Adv. Phys. *1* (1952) 1.
25. *Buck, O.:* phys. stat. sol. *2* (1962) 535.
26. *Blewit, T. H.; Coltmann, R. R; Rebstock, J. K.:* Phil. Mag. *2* (1957) 323.
27. *Verhoeven, J. D.; Spitzig, W. A.; Schmidt, F. A.; Krotz, P. D.; Gibson, E. D.:* J. Mater. Sci. *24* (1989) 1015.
28. *Courtney, T. H.:* in: D. Kuhlmann-Wilsdorf, W. C. Harrigan (eds.), New Developments and Applications in Composites, AIME, Warrendale, PA (1979) 6.
29. *Herlach, F.:* IEEE Trans. Magn. *24* (1988) 1049.

(Received August 16, 1994)